Articles in PresS. Am J Physiol Cell Physiol (June 11, 2014). doi:10.1152/ajpcell.00006.2014

Mitochondrial inefficiencies and anoxic ATP hydrolysis capacities in diabetic rat heart

Toan Pham[1], Denis Loiselle[2,3] , Amelia Power[1] and Anthony J.R Hickey[1]

[1]School of Biological Sciences the University of Auckland

[2]Faculty of Medical and Health Sciences and [3]Auckland Bioengineering Institute, the University of Auckland

Corresponding author Dr Anthony Hickey, email: a.hickey@auckland.ac.nz

Postal address: Thomas Building, 3 a Symonds Street, Applied Surgery and Metabolism, School of Biological Sciences, University of Auckland, New Zealand,

Running title: Diabetic heart mitochondrial efficiency

Copyright © 2014 by the American Physiological Society.

Abstract

As approximately 80% of diabetics die from heart failure, understanding diabetic cardiomyopathy is crucial. Mitochondria occupy 35-40% of the mammalian cardiomyocyte volume, supply 95% of the hearts' ATP, and diabetic heart mitochondria show impaired structure, arrangement and function. We predict that bioenergetic inefficiencies are present in diabetic heart mitochondria; therefore we explored mitochondrial proton and electron handling by linking oxygen flux to steady-state ATP synthesis, reactive oxygen species (ROS) production, and mitochondrial membrane potential ($\Delta\Psi$) within rat heart tissues. Sprague-Dawley rats were injected with either streptozotocin (STZ; 55 mg/kg) to induce Type I diabetes or an equivalent volume of saline (Control; n = 12) and fed with standard rat chow for eight weeks. By coupling high-resolution respirometers with purpose-built fluorometers, we followed Magnesium Green (ATP synthesis), Amplex Ultra Red (ROS production), and safranin-O ($\Delta\Psi$). Relative to Control rats, the mass-specific respiration of STZ-diabetic hearts was depressed in oxidative phosphorylating (OXPHOS) states. Steady-state ATP synthesis capacity was almost a third lower in STZ-diabetic heart and relative to O_2 flux, this equates to an estimated 12% depression in OXPHOS efficiency. However, with anoxic transition, STZ-diabetic and Control heart tissues showed similar ATP hydrolysis capacities through reversal of the F_1/F_0 ATP-synthase. STZ-diabetic cardiac mitochondria also produced more net ROS relative to oxygen flux (ROS/O) in OXP. While $\Delta\Psi$ did not differ between groups, the time to develop $\Delta\Psi$ with the onset of OXPHOS was protracted in STZ-diabetic mitochondria. ROS/O is higher in life-like OXPHOS states and potential delays in the time to develop $\Delta\Psi$ may delay ATP synthesis with inter-beat fluctuations in ADP concentrations. Whereas diabetic cardiac mitochondria produce less ATP in normoxia, they consume as much ATP in anoxic infarct-like states.

Abbreviations

ADP, adenosine diphosphate; ATP, adenosine triphosphate; AUR, amplex ultrared; Asc, ascorbate; Bleb, blebbistatin; CCO, cytochrome C oxidase; CI, complex I; CII, complex II; CE, cardiac efficiency; DC, diabetic cardiomyopathy; diabetic, diabetic mellitus; FCCP, carbonyl cyanide p-(trifluoromethoxy) phenol-hydrazone; GMP, glutamate+malate+pyruvate; HRP, horseradish peroxidase; LVH, left ventricular hypertrophy; MgG, magnesium green; NADH, nicotinamide adenine dinucleotide; O2k, oxygraph 2k; Oli, oligomycin; OXPHOS, oxidative phosphorylation; ROS, reactive oxygen species; S, succinate; SOD, superoxide dismutase; TCA, tricarboxylic acid cycle; TMPD, N,N,N',N'-tetramethyl-p-phenylenediamine.

Key words

Mitochondrial efficiency, ATP flux, mitochondrial membrane potential, mitochondrial ROS production.

Introduction

Diabetes mellitus constitutes a global epidemic and is most prevalent in developed countries, with the adult incidence predicted to increase over time (19, 37, 45). Clinical and experimental studies have associated diabetes with atherosclerosis of the arterial tree (including coronary arteries), and this increases the risk of limb loss through gangrene, stroke and myocardial infarction leading overall likelihood of developing heart failure (1, 8, 10, 19, 26).

Mechanisms that are independent of coronary artery disease and hypertension appear to promote heart failure in diabetic patients. Rubler *et al*. (64) coined the term "diabetic cardiomyopathy" noting that while diabetic patients had apparently normal coronary vasculature, they had abnormal ventricle structure and function independent of coronary artery disease and hypertension (22). Diabetic cardiomyopathy manifests with left ventricular hypertrophy (LVH), an increased susceptibility to ischemic injury and altered myocardial structure, Ca^{2+} homeostasis and cardiac substrate metabolism (2, 5, 7, 11, 17, 40).

Sustained heart function is dependent on aerobically derived ATP to fuel contraction. Approximately 95% of this ATP comes from mitochondrial oxidative phosphorylation systems (OXPHOS). Diabetic hearts show progressive declines in cardiac contractile efficiency alongside changes in metabolism (13). However, reports on changes in terms of metabolic efficiency, i.e. the conservation of energy from substrate oxidation to ATP production, are varied, with some studies reporting increased proton leak in diabetic rat heart mitochondria (decreased efficiency) (1, 11, 12, 57, 60), yet with similar P/O ratio to non-diabetic mitochondria (57). We note that these efficiency measures were conducted with standard equipment and protocols that may not have fully stressed mitochondria or have had the resolution to detect differences in efficiencies in steady state respiring mitochondria.

We predict that there are three points of potential energy loss: 1) ATP synthesis efficiency (tested by following ATP output and oxygen flux), 2) mitochondrial membrane potential ($\Delta\Psi$) and resulting dynamics with transitions between levels or degrees of phosphorylating respiration, and 3) the loss of electrons from the electron transport system (ETS) through the production of reactive oxygen species (ROS). Here we explore streptozotocin (STZ)-induced diabetes in Sprague Dawley rat heart homogenates and real-time measurements of these three parameters simultaneously with respirational flux by coupling purpose-built fluorometers to high resolution respirometers.

Methods

Animals

Male Sprague–Dawley rats (250-300g) were randomly assigned to two groups: STZ-induced diabetic (injected with 55 mg STZ/kg, henceforth called 'diabetic') and Control (injected with an equivalent volume of saline) (n=12 for both groups). Animals were housed in pairs (12 hr light-dark cycle, 50-70% humidity and 19-21°C) and fed standard rat chow and tap water *ad libitum* for eight weeks. Blood glucose levels and body weights were monitored daily in the first week and weekly thereafter. All studies were approved by the Animal Ethics Committee of the University of Auckland (R925). All chemicals were sourced from Sigma-Aldrich (MO, USA).

Sample preparation

Animals were anaesthetised with isofluorane until unresponsive to pinching the hindfeet. Following cardiotectomy, the LV was cut into small pieces, and transferred into 1 mL cold HTK transplant buffer (Histidine-Trypophan-Ketoglutarate, Custodial®, Alsbech Hähnlein, Germany). Of the three distinct experimental preparations available: isolated mitochondria,

96 permeabilised fibres and tissue homogenates, we utilise homogenates to test cardiac
97 mitochondrial function for reasons discussed extensively elsewhere (38).

98 Approximately 20 mg of LV tissue was weighed and transferred into 500 µL of ice-cold
99 incubation assay medium (for details, refer to (68)), homogenized for 15 s using a tissue
100 homogenizer (Omni International, Georgia, USA) and loaded immediately into the oxygraph
101 (1mg mL^{-1}).

102 **High resolution respirometry**

103 Three Oroboros Oxygraph 2k (O2k, Oroboros Instruments, Innsbruck, Austria) were
104 employed for all measurements of mitochondrial respiration fluxes (34). The O2k consists of
105 two independent 2 mL chambers with polarographic oxygen sensors and stoppers that allow
106 substrate inhibitor titrations. A purpose-built detachable fluorometer was inserted into each of
107 the front two windows of the O2k chambers to measure fluorescence of different
108 fluorophores (42). The O_2 concentration of the assay medium was 195 nmol O_2/mL at 95 kPa
109 barometric pressure. All experiments were performed at 37°C.

110 **Mitochondrial Respiration assays**

111 Titration protocols of multiple substrates and inhibitors were used to assess mitochondrial
112 function in terms of different respiration states. Complex I (CI)-mediated "Leak" respiration
113 was determined using malate, glutamate and pyruvate. The addition of succinate was then
114 used to reduce FAD at Complex II (CII, via succinate dehydrogenase) and saturating ADP
115 was added to stimulate OXPHOS. The Leak rate with CI and CII was determined before ADP
116 addition, and after with oligomycin to block the F_1F_0-ATPase, which was then followed with
117 repeated FCCP titrations to uncouple and depolarise the mitochondria (43). The addition of
118 antimycin A inhibited complex III (CIII), resulting in non-mitochondrial respiration with

small contributions from electron Leak in the uncoupled state. Further details of protocols are described in Goo *et al*. (38).

Protocol 1: Measurement of ATP production in cardiac homogenates

ATP/ADP exchange was measured by following Magnesium Green (MgG) fluorescence using excitation and emission wavelengths at 503 nm and 530 nm, respectively (20). ATP assays were conducted using our standard respiration buffer $MiRO_5$, which contains 3 mM $MgCl_2$. MgG (5 μM) was added to media together with ouabain (0.03 mM), to inhibit the Na^+/K^+ ATPase, and blebbistatin (0.05 mM) as an inhibitor of the myosin heavy-chain (48). Oxygen was added to the chamber header spaces prior to commencing the assay to super-saturation media to prolong the assay. Exactly 2 mg of tissue (approximately 50 μL of homogenate) was added into the chambers and allowed to equilibrate. CI Leak was determined using 2 mM malate, 10 mM glutamate and 10 mM pyruvate. CI and CII-mediated Leak was then assessed by addition of 10 mM succinate. At this point, excess Mg^{2+}-free ADP (2.5 mM) was added, to stimulate OXPHOS, and ATP production measured. Both CI and CII substrates were added prior to ADP as this state better reflects *in vivo* ETS electron input (59). The tissue was then allowed to respire into anoxia where there was an apparent decrease in ATP (i.e., ATP was hydrolysed). The addition of oligomycin (5 μM) returned the ATP production/hydrolysis rate to near 0. These data indicate that the F_1F_0-ATPase accounts for the majority of ATP hydrolysis in anoxia.

To calibrate the ATP signal, independent assays were performed without sample, and Mg^{2+} free-ADP or ATP was titrated stepwise (1.25, 2.5, 3.75, 5 and 6.25 mM). ADP and ATP calibration curves were constructed and the ratio of the slopes between the two calibration curves used to derive a fluorescence correction factor, which reflects the greater binding

affinity of ATP for Mg^{2+}. This correction factor was used to multiply the ADP signal, and to determine the ATP production rate (38).

Protocol 2: Measurement of mitochondrial membrane potential

Safranine-O was used to measure the ΔΨ fluorimetrically with excitation and emission wavelengths of 530 nm and 590 nm, respectively. Safranine (2 μM) was added to each chamber and allowed to equilibrate before adding 50 μL of homogenate containing 2 mg of LV tissue. CI and CII substrates (malate, glutamate, pyruvate and succinate, as above) were supplied for mitochondrial respiration. Once the safranine signal had stabilised, excess ADP (2.5 mM) was added to stimulate OXPHOS. The Leak state (CI and CII) was determined by addition of oligomycin (5 μM), followed with repeated titrations of FCCP (0.5 μM) to uncouple and depolarise mitochondria (43). The addition of antimycin A (5 μM) inhibited CIII and respiration. The addition of further safranine (1 μM) to the chamber, in the presence of the tissue sample and all titrated compounds, was used to normalise the safranine signal.

While calibration of the safranine signal can be performed by clamping and titration of KCl in the presence of the K^+ ionophore valinomycin, $MiRO_5$ (the buffer used in this present study) contains high K^+. We used an alternative approach to estimate ΔΨ. A near linear relationship between change of safranine fluorescence and ΔΨ has been reported, thereby allowing the estimation of ΔΨ (28). Approximately 35-40% of the cardiomyocyte volume is occupied by mitochondria (6). The mitochondrial matrix volume in transitions between OXPHOS and Leak states is dynamic, accounting for 29% and 44% of the mitochondrial volume, respectively (47). We therefore estimate matrix volumes to be 0.2 and 0.31 μL/mg of tissue in respective OXPHOS and Leak states. In consequence, the fluorescence from a known safranine concentration can be used to estimate the safranine in the media and that imported into the mitochondrial matrix (as is conducted using TPP^+). Using the Nernst

Equation, $\Delta\Psi = RT/zF\ ln([Safranine]_{out}/[Safranine]_{in})$, where R is the gas constant, F is the Faraday constant, T is temperature (K) and z is the valence state of the ion (+1). $[Safranine]_{out}$ and $[Safranine]_{in}$ are the respective safranine concentrations outside and inside the mitochondrial matrix.

Protocol 3: Net production of reactive oxygen species (ROS)

The superoxide radical ($O_2^{\cdot-}$) is formed from molecular oxygen as a by-product of oxidation at mitochondrial CI and CIII. *In vivo*, it is normally degraded by superoxide dismutases (SOD) to H_2O_2, or consumed by antioxidants and antioxidant enzyme systems, and is generally further reduced to O_2 and H_2O by peroxidases and catalase *in vivo* (54).

The net ROS production was measured simultaneously with respirational flux using Amplex Ultrared (AUR) dye. $O_2^{\cdot-}$ released from mitochondria was reduced to form H_2O_2 by addition of exogenous SOD. The combined mitochondrial H_2O_2 and exogenous SOD-derived H_2O_2 was then linked to horseradish peroxidase (HRP), which in turn reacts with AUR to form a fluorescent product with excitation and emission wavelengths of 530 nm and 590 nm respectively.

AUR (5 μM), SOD (10 U) and HRP (10 U) were added to the chambers, followed by H_2O_2 (330 nM), to calibrate the ROS signal. Homogenate (2 mg of wet tissue) was added into the chambers and allowed to equilibrate. CI and CII substrates were supplied to initiate the Leak state. Addition of ADP (2.5 mM) stimulated OXPHOS. The Leak rate with CI and CII was again determined by addition of oligomycin (5 μM) and then followed with repeated titrations of FCCP (0.5 μM) to uncouple mitochondria. Addition of antimycin A (5 μM) was added and the activity of cytochrome c-oxidase (CCO) was measured using the electron donor couple TMPD (0.5 mM) and ascorbate (2 mM).

Citrate synthase (CS) assay

Citrate synthase was used to provide an estimator of mitochondrial mass. Frozen tissues (- 80 °C) were thawed, minced, weighed, and homogenized in 1:10 (wt/vol) ice-cold buffer consisting of (in mM): 25 Tris-HCl at pH 7.8, 1 EDTA, 2 $MgCl_2$, 50 KCl and 0.50% v/v Triton X-100. The tissue homogenates were centrifuged at 14,000 *x* g for 10 min at 4^{o}C (Eppendorf Centrifuge 5417R) and the supernatant was frozen for CS assays (55). CS activities were determined following Sere, (67) based on the slope (Δ absorbance/Δ min) and activities were standardized to purified CS.

Data analysis

All data are presented as mean ± standard error (SE). Student t-tests (2-tailed) were performed using either Excel or Sigma Plot version 11.0 (Systat Software, Inc., San Jose, CA) to test the differences between Diabetic and Control groups, with $P < 0.05$ considered to be statistically significant; in figures and tables the following convention is adopted *$P < 0.05$, **$P < 0.01$ and ***$P < 0.001$. Each data point arose from replicated independent experiments.

Results

Physiological parameters of the Diabetic model

Blood glucose levels and body weights were measured weekly for all animals. Two days after STZ-injection the rats developed diabetic symptoms such as high blood glucose (>20 mM), polydipsia and polyuria. On average, the blood glucose levels remained almost four times higher, and the average body weight was significantly lower, in the Diabetic group, 8 weeks post-injection (Table 1). No statistical difference was detected in the average LV free-wall

thickness but, when expressed as a ratio of heart wet weight, the STZ diabetic rats had a greater relative LV thickness.

Mitochondrial respiration

Respirational flux in CI+II Leak, OXPHOS and ETS states in the ROS, ΨΔ and ATP-assays were consistently higher in the Control relative to the Diabetic groups (Figure 1a), indicating an overall depression in respiration capacities in diabetes. The Diabetic tissue homogenates showed no significant difference in respiratory control ratio (RCR CI+II) relative to Control LV homogenates. Addition of the uncoupling agent FCCP led to a higher relative maximal flux rate and higher UCR (ETS/OXPHOS) in the Control group relative to the Diabetic group (Table 2*)*, indicating that the untreated mitochondria were more tightly controlled by the phosphorylation system and had greater reserve ETS capacities. The CCO flux was 16% lower in the Diabetic group ($P = 0.07$).

The mitochondrial enzyme citrate synthase (CS) was assayed in homogenates as a marker for mitochondrial content. CS activities did not differ significantly between the Control and Diabetic groups, 9.30 ± 0.79 and 8.29 ± 0.37 $\mu mol.min^{-1}$ mg^{-1} wet weight, respectively ($P > 0.05$). The trends of respirational fluxes normalised to CS (Figure 1b) resembled those determined relative to mass indicating that the depression in mitochondrial respirational flux mostly results from qualitative differences in mitochondria, and are less due to decreased mitochondrial mass.

Steady-state ATP synthesis measurements

The Diabetic group also showed a 40% depression in mass specific ATP production rates (Figure 2b). When presented relative to steady-state oxygen flux, we observed a significantly lower P/O ratio as a measure of mitochondrial phosphyration efficiency (Figure 2c). In this experiment we permitted respiration to continue into anoxia and then observed a reversal in

the ATP flow signal (Figure 2a). Following addition of oligomycin, the ATP hydrolysis was mostly inhibited, indicating that hydrolysis was occurring at the F_1/F_0-ATP synthase. In contrast to ATP production rates, ATP consumption rates in anoxia were equivalent in Diabetic and Control groups (Figure 2b).

Membrane potential

$\Delta\Psi$ in the Leak state reached similar estimated resting voltages of -197 ± 6 mV (n = 8) in Control group and -207 ± 3 (n = 8) in Diabetic group and, with the onset of OXPHOS, reached similar voltages (-170 mV (static) to -180 mV (dynamic)) in both groups, depending on matrix volume model (Figure 3a). Diabetic mitochondria, however, took longer to depolarize with the initiation of OXPHOS, indicating a slower response to elevated OXPHOS and, therefore, a decreased rate of ATP synthesis in diabetic hearts (Figure 3b).

ROS production

The mass specific production of ROS was considerably higher in the Leak states than in the OXPHOS states regardless of disease status (Figure 4a). Diabetic group produced substantially less ROS than Control mitochondria in leak respiration states, but similar rates in OXPHOS. Given the differences in respiration capacities, ROS production was presented relative to oxygen flux. The diabetic mitochondria exhibited higher ROS/O ratio, indicating a greater leakage of ROS relative to oxygen consumption under physiological OXPHOS respiration states (Figure 4b).

Discussion

Our collective evidence indicates that diabetic cardiac mitochondria are less efficient than those from untreated hearts. They produce less ATP in normoxic steady-state respiration states and release marginally more ROS per oxygen consumed in OXPHOS states. They also

take longer to modulate ΔΨ with fluctuations in ADP (i.e. as may occur between heart beats). Our most important observation is that, despite substantial depression of ATP synthesis capacity in oxygen saturated states, diabetic heart mitochondria appear to consume as much ATP in anoxic infarct-like states as mitochondria from healthy hearts.

With development of diabetic cardiomyopathy, structural and metabolic alterations impact the myocardium and contribute to cardiac dysfunction (8, 56). A relative increase of 24% of the LV thickness/ heart weight (HW) ratio (Table 1) was apparent and this is consistent with published data for STZ-induced diabetic rats hearts, which progressively show depressed pumping capacities (52), most likely through decreasing LV compliance (4). We note that contemporaneous work found decreased pumping efficiencies at elevated afterloads in the same source of rats as used in this present study (39). A significant decrease in heart rate (15%) and increase in systolic duration (24%) also occurs in the 8-weeks STZ-diabetic Wistar rats (52), and has been reported in diabetic men and women (22).

Multiple substrate and inhibitor titrations were used to maximise the flux in various respiration states in an attempt to mirror electron flow in substrate-saturated cardiomyocytes at high work-loads. Mass-specific, ADP-stimulated, coupled respiration (OXPHOS) with parallel CI and CII electron inputs was decreased by 24% in the Diabetic group when expressed per unit of tissue mass (Figure 1a), which is consistent with reports of decreased mitochondrial activities in diabetic heart (44). Normalization of mitochondrial respiration to citrate synthase (CS) activity to distinguish changes in mitochondrial density(49), showed no statistical difference in CS activities between groups. This indicates that depression of mitochondrial function likely results from decreased capacities of the diabetic mitochondria.

The OXPHOS uncoupler FCCP, which dissipates ΔΨ, generally maximises respiration through the ETS (59). We note a slight depression in ETS flux relative to OXPHOS and

282 contend that the loss of ΨΔ may result from decreased electrogenic substrate import. Here we
283 present the uncoupling control ratio (UCR) or E/P as the relative of ETS capacity normalized
284 to OXPHOS. Assuming that the influence of FCCP is equal between the two groups, we note
285 that the UCR is 19% more depressed in diabetic samples. This depression may result from
286 one or more of the following: a relative insufficiency of the ETS, a proportionate increase in
287 ATP-synthase capacity, or increased proton leak (29, 51).

288 The contribution of CII-derived flux to Leak respiration was 26% higher in the Control group
289 relative to the Diabetic group, indicating an intrinsic difference in ETS function (Table 2).
290 Some investigators contend that CII mediated respiration may elevate ATP output rates at a
291 cost to efficiency (30). The lower fraction of CII contribution to Leak respiration in Diabetic
292 mitochondria would predict greater phosphorylation efficiencies in OXPHOS, however we
293 detected lower ATP production rates in Diabetic group.

294 In accord with previous work (53), our findings show that respirational function is depressed
295 in the diabetic heart. This also results in a depression of cytochrome-c oxidase (CCO)
296 activity, the terminal step of the ETS where O_2 is reduced to H_2O. CCO flux generally
297 appears to be in excess capacity relative to the ETS flux in most mitochondria (36), and is
298 more so in cardiac mitochondria relative to other tissues such as liver (9). While mass
299 specific CCO flux was substantially higher (16%) in Control rats compared to Diabetic rats
300 (Figure 1a), the CCO flux presented as that relative to OXPHOS and ETS (i.e.
301 CCO/OXPHOS, CCO/ETS) was conserved between groups, and therefore differences in
302 CCO flux relates to differences in mitochondrial mass (35). Lower overall capacities of CCO
303 in diabetic mitochondria may decrease O_2 uptake at low oxygen tensions and/or enhance the
304 effect of NO, a potent inhibitor of CCO (33), which is known to increase with
305 hyperglycaemia (21).

306 The RCR, which is the inverse of the Leak ratio, is widely used to evaluate the structural
307 integrity of the inner mitochondrial membrane and OXPHOS efficiency (30). The RCR is
308 perhaps less informative, since the Leak/OXPHOS ratio provides a more direct index of the
309 fraction of Leak respiration not contributing to OXPHOS. The Leak control ratios as CI+CII
310 Leak / CI+CII OXPHOS in the ROS-assay were approximately 20-25%. While this appears
311 high relative to leak fluxes for CI-fuelled respiration (7-10% (32, 61)), it reflects the lesser
312 proton pumping capacity of CII electron transport chains. Here the RCR values did not differ
313 between groups in the present study. However, phosphorylation efficiencies may be dynamic,
314 as mitochondria with high apparent Leak rates (or low RCRs) can show P/O ratios similar to
315 those with low Leak ratios (high RCRs) (59). This may result from experimental variability,
316 and/or the estimation of P/O ratios in non-steady states from single substrates.

317 **Steady-state ATP synthesis measurements**

318 Here we present P/O ratios in steady state respiration states, which attempt to maximise the
319 loading on mitochondria through use of multiple electron inputs. Diabetic mitochondria were
320 less efficient. ATP synthesis efficiency can be altered due to proton Leakage through ANT,
321 UCPs and directly through the inner mitochondrial membrane (14). The steady-state P/O
322 ratio derived in this study contrasts with those measured using isolated mitochondria and
323 traditional extrapolation of traces for deriving OXPHOS efficiencies (57). We consider that
324 these differences can be attributed to our real-time measurements of ATP synthesis in steady-
325 states at sustained high flux rates, and the use of multiple electron inputs in the titration
326 protocol.

327 The stoichiometry of proton translocation across the inner mitochondrial membrane (IMM)
328 can be used to determine the steady-state P/O ratio. The maximum P/O ratio for CI and CII
329 substrates is predicted to be ~2.5-2.8 and 1.5 respectively (50). The steady-state P/O ratio is

calculated from the following identity: P/O ratio = $P/O_{max} \cdot J_p/J_s$, where J_p and J_s are the fluxes through the phosphorylation and substrate modules, respectively (15). Proton leakage and the addition of less OXPHOS coupled CII substrates to CI substrates should decrease the P/O ratio (25).

The steady-state P/O ratio with CI and CII substrates in this study provides a useful understanding of ATP synthesis and turnover. With both CI and CII assayed together the P/O ratio should be intermediate to 2.5-2.8 and 1.5 and we observed P/O ratios of ~2 in healthy heart. This approximates the P/O ratios of Langendorff-perfused hearts using 31P NMR supported by pyruvate (~2.1, (46)). The steady-state P/O ratios were 18% lower in Diabetic rats (Figure 2c), indicating decreased mitochondrial coupling, which associates with decreased cardiac efficiency (17). While standard methods predicted decreased P/O ratios in db/db type II diabetic mice (13) and UCP-DTA mice (27), others have also demonstrated unchanged, if not improved P/O ratios in mitochondria isolated from 8 week STZ-diabetic rats (41). Although similar in diabetic exposure to this present study, our study did not isolate mitochondria, with the aim to retain all mitochondrial populations. Importantly we measured ATP synthesis in real time with abundant ADP, and both complex I and II electron inputs, as must occur *in vivo* in hard working hearts. The absolute ATP output is 35% less per gram in diabetic hearts (Figure 2b), and this should decrease high-energy phosphate supplies at high workloads in diabetic hearts.

By measuring ATP in real-time we could also measure adenylate dynamics in anoxia. An imbalance between ATP production and consumption was apparent in diabetic mitochondria. Diabetic human hearts are more susceptible to ischemic insults, as are rodent hearts following prolonged diabetes (58). Under anoxia, mitochondria stop electron transport and decrease proton pumping across the IMM. When the $\Delta\Psi$ is thought to dissipate to ~-100 mV, the ATP-synthase activity reverses and ATP-hydrolase activity dominates (24). While a lower rate of

ATP production occurred in diabetic tissues, there was no significant difference of oligomycin-sensitive ATP consumption between diabetic and normal rat homogenates (Figure 2b). Oligomycin addition shows that the hydrolytic activity of the diabetic rat heart ATP-synthase can consume similar amounts of ATP in anoxia, but cannot make the same amount of ATP in normoxia. These data provide a potential mechanism for the poor recovery of diabetic hearts from ischemic insults.

Mitochondrial membrane (ΔΨ) potential

Based on a known safranine fluorescence signal, we estimated ΔΨ. As safranine is a lipophilic cationic dye, it may bind within the mitochondrial matrix independent of ΔΨ. This binding coefficient is unavailable, and may lead to overestimates of ΔΨ in the vicinity of -25 mV (63). In accordance, the maximal ΔΨ reported in this study was around -205 mV (Figure 3a). An overestimate of -25 mV would place this value at -180 mV, which is consistent with literature using tetraphenlyphosphonium (TPP (31)).

The mitochondrial volume is approximately 40% of that of a cardiomyocyte. The matrix volume, which is not static, occupies 29% of the mitochondrial volume in the OXPHOS state, and can swell by 44% in Leak states and in hypoxia (47). ΔΨ was similar for both groups (Leak, -200 mV and OXPHOS, -170 mV). While these estimates are higher than those reported by others using different methods, the difference between states is similar (i.e.~30 mV(28, 69)). While it makes no apparent difference for comparisons between treatment groups, a dynamic matrix volume predicts shrinkage on transition to OXPHOS from the Leak state, and this increases the ΔΨ by 10 mV relative to OXPHOS in a static matrix model. This impacts current views of ROS production, which is assumed to be mediated by high ΔΨ (54).

While ΔΨ values did not differ between the groups, our ΔΨ assays were able to show that the time required for ΔΨ to reach a steady-state (t_s) was protracted in Diabetic samples with the

transition from Leak to OXPHOS (Figure 3b). Protracted t_s may reflect depressed respiration flux rates in diabetes, which impedes ΔΨ development. The development of ΔΨ not only mediates ATP production but also drives substrate import and Ca^{2+} uptake, which also stimulate TCA cycle dehydrogenases (16, 23). Delays in the establishment of ΔΨ may therefore influence ATP synthesis, substrate import/turnover and Ca^{2+} buffering and ROS production.

ROS production in diabetic cardiac mitochondria

One of the methodological advantages achieved in this study was the simultaneous measurement of ROS output (pmol/s/mg wet weight of tissue) and respirational flux, measured also in Leak and OXPHOS states. ROS generation from the ETS is assumed to be 0.1-4% of O_2 consumption (66). Our observations agree with others (41) as we demonstrate that H_2O_2 production in control specimens is greater in the CI + CII Leak state than diabetics, as was the % ROS/O (1.48%) group. However, while the H_2O_2 production rate was low in absolute terms, the ROS/O ratio in the OXPHOS state was 47% higher in Diabetic group (Figure 4b), and this state, unlike the Leak state is a physiologically relevant respiration state, with relevant electron inputs. Studies using a type I diabetes Akita mouse model and STZ-diabetic rats showed no evidence for increased mitochondrial ROS generation (18, 41), the range of ROS/O ratio in OXPHOS was 0.015 – 0.03%, which was also observed in a hypertensive, non-diabetic, rat heart failure model (43). While elevated relative to the control animals, whether this low amount of ROS can mediate damage in diabetic cardiomyopathy remains to be tested.

The CI and CII substrate combination elevates the electron inputs into ETS at ubiquinone and represents more realistic scenarios of ATP synthesis and ROS production. The high ΔΨ generated by CI+CII Leak is also thought to promote reverse electron transfer (RET) from

CII back to CI through ubiquinone (3). While mechanistically unclear, electron accumulation at the semi-quinone formation site within CI results in $O_2^{\cdot-}$ evolution (3). Whether RET occurs *in vivo* remains unanswered, however RET is dependent on mitochondrial coupling and ADP concentration (as shown in the current study and elsewhere(62)), and ROS production clearly declines in OXPHOS states. Mitochondria of healthy working hearts in normoxia are likely never completely ADP limited, and ROS measurement in the OXPHOS state is likely to be informative. However, as matrix ADP concentration fluctuates (16) so may ROS outputs. Moreover, mitochondrial creatine kinase decreases with diabetes (44) and this should impede ADP return to the matrix and potentially elevate ROS. Our study shows that while $\Delta\Psi$ is maintained at similar apparent levels in control and diabetic samples, protracted transitions of $\Delta\Psi$ from the high "near-Leak" to the lower OXPHOS $\Delta\Psi$ in diabetic groups could act to raise ROS.

Our measures of ROS in the Leak and OXPHOS states are net ROS production, i.e. the sum of production and removal. The elevated ROS/O ratio in the OXPHOS state in the diabetic group may be due to altered ETS function and/or impaired ROS defence systems. Electron-leakage from the ETS as $O_2^{\cdot-}$ is converted by SOD to H_2O_2, and further reduced to H_2O by systems such as glutathione peroxidase (GPX) (3). While SOD2 concentrations can increase by 45% in diabetic hearts (44), decreased reduced-glutathione (GSH) concentrations have been reported in diabetic hearts (65), suggesting that downstream consequences of increased ROS production and challenged detoxification systems occur in diabetic mitochondria (18).

Conclusions

Diabetic cardiac mitochondria respire and phosphorylate with less capacity and efficiency (ATP produced/O) than mitochondria from healthy hearts. ROS production relative to O is higher in diabetic samples in more life-like OXPHOS states. While minimal, this ROS

production represents a loss of electrons that otherwise could contribute to ATP synthesis. The protracted development of $\Delta\Psi$ may impair activation of ATP synthesis and elevate ROS with inter-beat fluctuations in ADP concentration. Perhaps most importantly, during anoxic infarct-like states, diabetic mitochondria appear to consume as much ATP as healthy hearts and this will possibly produce a greater ATP deficit on reoxygenation. This presents a possible mechanistic explanation for the susceptibility of diabetic hearts to infarct.

Acknowledgements

We would like to thank Amorita Petzer for assistance with help with animal husbandry and Dr Bernard Cheung for training assistance. We would also like to thank Nicholas Pearson for help with assay development. This work was funded by grants from the Health Research Council of New Zealand (11/585), the National Heart Foundation of New Zealand (*Small Project Grants* No 1428 and No 1529), the Maurice and Phyllis Paykel Trust (University of Auckland Project Number 3701355).

References

1. **Aasum E, Belke D, Severson D, Riemersma R, Cooper M, Andreassen M, and al. e.** Cardiac function and metabolism in Type 2 diabetic mice after treatment with BM 17.0744, a novel PPARalpha activator. *Am J Physiol Heart Circ Physiol* 283: H949-957, 2002.
2. **Anderson E, Kypson A, Rodriguez E, Anderson C, Lehr E, and Neufer P.** Substrate-specific derangements in mitochondrial metabolism and redox balance in the atrium of the type 2 diabetic human heart. *J Am Coll Cardiol* 54: 1891-1898, 2009.
3. **Andreyev AY, Kushnareva YE, and Starkov AA.** Mitochondrial metabolism of reactive oxygen species. *Biochem Mosc* 70: 200-214, 2005.
4. **Aurigemma GP, Silver KH, Priest MA, and al. e.** Geometric changes allow normal ejection fraction despite depressed myocardial shortening in hypertensive left ventricular hypertrophy. *J Am Coll Cardiol* 26: 195–120, 1995.
5. **Ballinger SW.** Mitochondrial dysfunction in cardiovascular disease. *Free Radical Bio Med* 38: 1278-1295, 2005.
6. **Barth E, Stammler G, Speiser B, and Schaper J.** Ultrastructural quantitation of mitochondria and myofilaments in cardiac muscle from 10 different animal species including man. *J Mol Cell Cardiol Jul* 24: 669-681, 1992.
7. **Belke DD, Swanson EA, and Dillmann WH.** Decreased sarcoplasmic reticulum activity and contractility in diabetic db/db mouse heart. *Diabetes* 53 3201-3208, 2004.
8. **Bella JN, Devereux RB, Roman MJ, Palmieri V, Liu JE, Paranicas M, Welty TK, Lee ET, Fabsitz RR, and Howard BV.** Strong Heart Study Investigators. Separate and joint effects of systemic hypertension and diabetes mellitus on left ventricular structure and function in American Indians (the Strong Heart Study). *Am J Cardiol* 87: 1260–1265, 2001.
9. **Benard G, Faustin B, Passerieux E, Galinier A, Rocher C, Bellance N, Delage J-P, Casteilla L, Letellier T, and Rossignol R.** Physiological diversity of mitochondrial oxidative phosphorylation. *Am J Physiol* 291C: 1172–1182, 2006.
10. **Boudina S and Abel ED.** Diabetic cardiomyopathy revisited. *Circulation* 115: 3213-3223, 2007.
11. **Boudina S and Abel ED.** Mitochondrial uncoupling: a key contributor to reduced cardiac efficiency in diabetes. *Physiology* 21: 250-258, 2006.
12. **Boudina S, Sena S, O'Neill BT, Tathireddy P, Young ME, and Abel ED.** Reduced mitochondrial oxidative capacity and increased mitochondrial uncoupling impair myocardial energetics in obesity. *Circulation* 112: 2686-2695, 2005.
13. **Boudina S, Sena S, Theobald H, Sheng X, Wright JJ, Hu XX, Aziz S, Johnson JI, Bugger H, Zaha VG, Abel ED, Boudina S, Sena S, Theobald H, Sheng X, Wright JJ, Hu XX, Aziz S, Johnson JI, Bugger H, Zaha VG, and Abel ED.** Mitochondrial energetics in the heart in obesity-related diabetes: direct evidence for increased uncoupled respiration and activation of uncoupling proteins. *Diabetes* 56: 2457-2466, 2007.
14. **Brand MD.** The efficiency and plasticity of mitochondrial energy transduction. *Biochem Soc Trans* 33: 897-904, 2005.
15. **Brand MD, Harper ME, and Taylor HC.** Control of the effective P/O ratio of oxidative phosphorylation in liver mitochondria and hepatocytes. *Biochem J* 291: 739-748, 1993.
16. **Brown GC.** Control of respiration and ATP synthesis in mammalian mitochondria and cells. *Biochem J* 284: 1-13, 1992.
17. **Bugger H and Abel ED.** Mitochondria in the diabetic heart. *Cardiovasc res* 88: 229-240, 2010.
18. **Bugger H, Boudina S, Hu XX, Tuinei J, Zaha VG, Theobald HA, and al. e.** Type 1 diabetic akita mouse hearts are insulin sensitive but manifest structurally abnormal mitochondria that remain coupled despite increased uncoupling protein 3. *Diabetes* 57: 2924–2932, 2008.
19. **Cameron VA, Faatoese AF, Gillies MW, Robertson PJ, Huria TM, Doughty RN, Whalley GA, Richards MA, Troughton RW, Tikao-Mason KN, Wells EJ, Sheerin IG, and Pitama SG.** A cohort study comparing cardiovascular risk factors in rural Maori, urban Maori and non-Maori communities in New Zealand. *BMJ Open* 2, 2012.

20. **Chinopoulos C, Vajda S, Csanady L, Mandi M, Mathe K, and Adam-Vizi V.** A novel kinetic assay of mitochondrial ATP-ADP exchange rate mediated by the ANT. *J Biophys* 96: 2490-2504, 2009.
21. **Cosentino F, Hishikawa K, Katusic ZS, and Lüscher TF.** High glucose increases nitric oxide synthase expression and superoxide anion generation in human aortic endothelial cells. *Circulation* 96: 25-28, 1997.
22. **Devereux R, Roman M, Paranicas M, O'Grady M, Lee E, Welty T, Fabsitz R, Robbins D, Rhoades E, and Howard B.** Impact of diabetes on cardiac structure and function: the Strong Heart Study. *Circulation* 101: 2271-2276, 2000.
23. **Dorn GW and Maack C.** SR and mitochondria: Calcium cross-talk between kissing cousins. *J Mol Cell Cardiol Jul* 2: 2, 2012.
24. **Duchen MR.** Mitochondria in health and disease: perspectives on a new mitochondrial biology. *Mol Aspects Med* 25: 365-451, 2004.
25. **Dufour S, N., Rousse N, Canioni P, and Diolez P.** Top-down control analysis of temperature effect on oxidative phosphorylation. *Biochem J* 314: 743-751, 1996.
26. **Duncan JG.** Mitochondrial dysfunction in diabetic cardiomyopathy. *Biochim biophysic acta* 1813: 1351-1359, 2011.
27. **Duncan JG, Fong JL, Medeiros DM, Finck BN, and Kelly DP.** Insulin-resistant heart exhibits a mitochondrial biogenic response driven by the peroxisome proliferator -activated receptor-α/PGC-1α gene regulatory pathway. *Circulation* 115: 909-917, 2007.
28. **Figueira TR, Melo DR, Vercesi AE, and Castilho RF.** Safranine as a fluorescent probe for the evaluation of mitochondrial membrane potential in isolated organelles and permeabilized cells. *Methods Mol Cell Biol* 810: 103-117, 2012.
29. **Gledhill JR, Montgomery MG, Leslie AGW, and Walker JE.** How the regulatory protein, IF1, inhibits F1-ATPase from bovine mitochondria. *PNAS* 104: 15671–15676, 2007.
30. **Gnaiger E.** Capacity of oxidative phosphorylation in human skeletal muscle: New perspectives of mitochondrial physiology. *Int J Biochem Cell Biol* 41: 1837-1845, 2009.
31. **Gnaiger E.** Mitochondrial Pathways and Respiratory Control, edited by Innsbruck AOMP, 2011.
32. **Gnaiger E.** Mitochondrial pathways and respiratory control. (1st ed.), edited by Gnaiger E. Innsbruck: OROBOROS MiPNet Publications, 2007.
33. **Gnaiger E.** *Oxygen conformity of cellular respiration; a perspective of mitochondrial physiology. Through the lifecycle*. New York, 2003.
34. **Gnaiger E.** *Polarographic oxygen sensors, the oxygraph and high-resolution respirometry to assess mitochondrial function*: John Wiley & Sons, Inc., 2008.
35. **Gnaiger E, Lassnig B, Kuznetsov A, Rieger G, and Margreiter R.** Mitochondrial oxygen affinity, respiratory flux control and excess capacity of cytochrome c oxidase. *J Exp Biol* 201: 1129–1139, 1998a.
36. **Gnaiger E, Lassnig B, Kuznetsov AV, Rieger G, and Raimund M.** Mitochondrial oxygen affinity, respiratory flux control and excess capacity of cytochrome c oxidase. *J Exp Biol* 201: 1129–1139, 1998b.
37. **Go AS, Mozaffarian D, Roger VL, Benjamin EJ, Berry JD, Borden WB, Bravata DM, Dai S, Ford ES, Fox CS, Franco S, Fullerton HJ, Gillespie C, Hailpern SM, Heit JA, Howard VJ, Huffman MD, Kissela BM, Kittner SJ, Lackland DT, Lichtman JH, Lisabeth LD, Magid D, Marcus GM, Marelli A, Matchar DB, McGuire DK, Mohler ER, Moy CS, Mussolino ME, Nichol G, Paynter NP, Schreiner PJ, Sorlie PD, Stein J, Turan TN, Virani SS, Wong ND, Woo D, and Turner MB.** Executive summary: heart disease and stroke statistics--2013 update: a report from the American Heart Association. *Circulation* 127: 143-152, 2013.
38. **Goo S, Pham T, Han JC, Nielsen P, Taberner A, Hickey A, and Loiselle DS.** Multiscale Measurement of Cardiac Energetics. *Clin Exp Pharmacol Physiol* 44: 2013-2003, 2013.
39. **Han J-C, Tran K, Nielsen PM, Taberner AJ, and Loiselle DS.** Streptozotocin-induced diabetes prolongs twitch duration without affecting the energetics of isolated ventricular trabeculae. *Cardiovascular Diabetology* 13: 79, 2014.
40. **Hayat SA, Patel B, Khattar RS, and Malik RA.** Diabetic cardiomyopathy: mechanisms, diagnosis and treatment. *Clin Sci (Lond)* 107: 539-557, 2004.

41. **Herlein JA, Fink BD, O'Malley Y, and Sivitz WI.** Superoxide and respiratory coupling in mitochondria of insulin-deficient diabetic rats. *Endocrinol* 150: 46–55, 2009.
42. **Hickey AJ, Renshaw GM, Speers-Roesch B, Richards JG, Wang Y, Farrell AP, and Brauner CJ.** A radical approach to beating hypoxia: depressed free radical release from heart fibres of the hypoxia-tolerant epaulette shark (*Hemiscyllum ocellatum*). *J Comp Physiol B* 182: 91-100, 2012.
43. **Hickey AJR, Chai CC, Choong SY, Costa SdF, Skea GL, Phillips ARJ, and Cooper GJS.** Impaired ATP turnover and ADP supply depress cardiac mitochondrial respiration and elevate superoxide in nonfailing spontaneously hypertensive rat hearts. *Am J Physiol Cell Physiol* 297, 2009.
44. **Jullig M, Hickey A, Middleditch M, Crossman D, Lee S, and Cooper G.** Characterization of proteomic changes in cardiac mitochondria in streptozotocin-diabetic rats using iTRAQ isobaric tags. *J Proteomics Clin Appl* 1: 565-576, 2007.
45. **King H, Aubert RE, and Herman WH.** Global burden of diabetes, 1995-2025: prevalence, numerical estimates, and projections. *Diabetes care* 21: 1414-1431, 1998.
46. **Kingsley-Hickman PB, Sako EY, Ugurbil K, From AH, and Foker JE.** 31P NMR measurement of mitochondrial uncoupling in isolated rat hearts. *J Biol Chem* 265: 1545-1550., 1990.
47. **Kjaerulf-Jensen H, Korsgaard N, Lindeberg H, and Vigholt-Sørensen E.** Myocardial ultrastructure in the isolated rabbit heart exposed to dopamine, dobutamine, isoprenaline, G-strofanthin, xamoterol and hypoxia. *Pharmacol Toxicol* 71: 302-304, 1992
48. **Kovacs M, Toth J, Hetenyi C, Malnasi-Csizmadia A, and Sellers JR.** Mechanism of blebbistatin inhibition of myosin II. *J Bio Chem* 279: 35557-35563, 2004.
49. **Larsen S, Nielsen J, Hansen CN, Nielsen LB, Wibrand F, Stride N, Schroder HD, Boushel R, Helge JW, Dela F, and Hey-Mogensen M.** Biomarkers of mitochondrial content in skeletal muscle of healthy young human subjects. *Physiology* 590: 3349-3360, 2012.
50. **Lee CP, Gu Q, Xiong Y, Mitchell RA, and Ernster L.** P/O ratios reassessed: mitochondrial P/O ratios consistently exceed 1.5 with succinate and 2.5 with NAD-linked substrates. *FASEB J* 10: 345-350, 1996.
51. **Lemieux M, Semsroth S, Antretter H, Ho□fer D, and Gnaiger E.** Mitochondrial respiratory control and early defects of oxidative phosphorylation in the failing human heart. *Int J Biochem Cell B* 43: 1729–1738, 2011.
52. **MacDonald JR, Oellermann M, Rynbeck S, Chang G, Ruggiero K, Cooper GJ, and Hickey AJ.** Transmural differences in respiratory capacity across the rat left ventricle in health, aging, and streptozotocin-induced diabetes mellitus: evidence that mitochondrial dysfunction begins in the subepicardium. *Am J Physiol Cell Physiol* 300: C246-255, 2011.
53. **MacDonald JR, Oellermann M, Rynbeck S, Chang G, Ruggiero K, Cooper GJS, and Hickey AJR.** Transmural differences in respiratory capacity across the rat left ventricle in health, aging, and streptozotocin-induced diabetes mellitus: evidence that mitochondrial dysfunction begins in the subepicardium. *Am J Physiol-Cell Ph* 300: C246-C255, 2011.
54. **Murphy M.** How mitochondria produce reactive oxygen species. *Biochem J* 417: 1-13, 2009.
55. **Newsholme EA and Crabtree B.** Maximum catalytic activity of some key enzymes in provision of physiologically useful information about metabolic fluxes. *J Exp Zool* 239: 159-167, 1986.
56. **Palmieri V, Bella JN, Arnett DR, Liu JE, Oberman A, Schuck M-Y, Kitzman DW, Hopkins PN, Morgan D, Rao DC, and Devereux RB.** Effect of type 2 diabetes mellitus on left ventricular geometry and systolic function in hypertensive subjects: Hypertension Genetic Epidemiology Network (HyperGEN) Study. *Circulation* 103: 102-107, 2001.
57. **Parks RE, Adler J, and Copenhaver JH.** The efficiency of oxidative phosphorylation in mitochondria from diabetic rats. *J Biol Chem* 214: 693-698, 1955.
58. **Paulson DJ.** The diabetic heart is more sensitive to ischemic injury. *Cardiovas Res* 34: 104-112, 1997.
59. **Pesta D and Gnaiger E.** High-resolution respirometry: OXPHOS protocols for human cells and permeabilized fibers from small biopsies of human muscle. *Methods Mol Cell Biol* 810: 25-58, 2012.
60. **Pierce GN and Dhalla N.** Heart mitochondrial function in chronic experimental diabetes in rats. *Can J Cardiol* 1, 1985.

61. **Rolfe DF and Brown GC.** Cellular energy utilization and molecular origin of standard metabolic rate in mammals. *Physiol Rev* 77: 731–758, 1997.
62. **Rolo AP and Palmeira CM.** Diabetes and mitochondrial function: role of hyperglycemia and oxidative stress. *Toxicology and applied pharmacology* 212: 167-178, 2006.
63. **Rottenberg H.** Membrane potential and surface potential in mitochondria: uptake and binding of lipophilic cations. *J Membr Biol* 81: 127-138, 1984.
64. **Rubler S, Dlugash J, Yuceoglu Y, Kumral T, Branwood A, and Grishman A.** New type of cardiomyopathy associated with diabetic glomerulosclerosis. *Am J Cardiol* 30: 595- 602, 1972.
65. **Shen X, Zheng S, Thongboonkerd V, Xu M, Pierce Jr WM, Klein JB, and Epstein PN.** Cardiac mitochondrial damage and biogenesis in a chronic model of type I diabetes. *Am J Physiol Endocrinol Metab* 287: E896-E905, 2004.
66. **Speakman JR, Talbot DA, Selman C, Snart S, McLaren JS, Redman P, Krol E, Jackson DM, Johnson MS, and Brand MD.** Uncoupled and surviving: individual mice with high metabolism have greater mitochondrial uncoupling and live longer. *Aging Cell* 3: 87-95, 2004.
67. **Srere P.** Citrate synthase. *Methods Enzymol* 13, 1969.
68. **Veksler VI, Kuznetsov AV, Sharov VG, Kapelko VI, and Saks VA.** Mitochondrial respiratory parameters in cardiac tissue: a novel method of assessment by using saponin-skinned fibers. *Biochimic Biophys Acta* 892: 191-196, 1987.
69. **Zukiene R, Nauciene Z, Ciapaite J, and Mildaziene V.** Acute temperature resistance threshold in heart mitochondria: Febrile temperature activates function but exceeding it collapses the membrane barrier. *Int J Hyperthermia* 26: 56-66, 2010.

627

628 **Figure legends**

629 **Figure 1: Mitochondrial respiration capacities in different respiration states of diabetic**
630 **(black) and age matched control hearts (open). (a)** Oxygen flux capacities per wet mass of
631 cardiac homogenate were derived from ROS experiments. **(b)** Capacity relative to citrate
632 synthase of 8-week diabetic rat hearts (black) and their age-matched controls (open). Leak CI
633 (non-phosphorylating flux) was initiated with Complex I (CI) substrates glutamate, malate
634 and pyruvate and Leak CI+II represents the leak respiration attributable to both CI and the
635 Complex II (CII) substrate succinate. After addition of ADP, oxidative phosphorylation flux
636 (OXPHOS) was measured. Leak CI+II was again measured after addition of oligomycin
637 (Leak o). The mitochondria were uncoupled with FCCP (uncoupled). Antimycin A was
638 added to inhibit Complex III and oxidative flux was measured through cytochrome c oxidase
639 (CCO) following TMPD and ascorbate addition. Paired student t-tests were used to test
640 statistical significant difference between the Control and Diabetic groups (* $P < 0.05$, ** $P <$
641 0.01, *** $P < 0.005$, $n = 12$ for both groups).

642 **Figure 2: ATP production capacities per milligram of diabetic (black) and age matched**
643 **control hearts (open). (a)** Simultaneous measurement of mitochondrial O_2 flux (not shown)
644 and ATP production. Respirational flux was followed in the presence of oxygen and CI and II
645 substrates (inset a, GMP-glutamate, malate, pyruvate and succinate) and then Mg^{2+}-free ADP
646 was added to initiate ATP synthesis (OXPHOS). Respiration was allowed to run into anoxia
647 after which oligomycin (Oli) was added and the background ATP hydrolysis signal
648 subtracted as background. **(b)** Rate of ATP production per mass of tissue (pmol/s/mg) in
649 normoxia and anoxia state. **(c)** The active, or steady-state P/O ratio was then determined from
650 the rate of ATP synthesised relative to the flux of molecular O in OXPHOS. (* $P < 0.05$, ** P

651 < 0.01, *** P < 0.005, n = 12 per group 8-week diabetic rat hearts and their age-matched
652 Controls).

653 **Figure 3: Mitochondrial membrane (ΔΨ) potential of diabetic (black) and age matched**
654 **control hearts (open). (a)** Estimated ΔΨ in Leak CI+CII and OXPHOS states. ΔΨ for both
655 fixed (44%) and dynamic (29%) matrix volume models are presented. **(b)** The time durations
656 required for ΔΨ to reach steady states of OXPHOS indicate a longer transition times occur
657 for diabetic heart mitochondria (* P < 0.05, n = 10 per group 8-week diabetic rat hearts and
658 their age-matched Controls).

659 **Figure 4: Reactive oxygen species (ROS) production of diabetic (black) and age**
660 **matched control hearts (open). (a)** Mean H_2O_2 (pmol H_2O_2 $(s.mg)^{-1}$) calibrated with a
661 known amount of H_2O_2 in various mitochondrial states. **(b)** The [ROS]/[O] ratio was indexed
662 as the amount of ROS production relative to respiration O flux (* P < 0.05, n = 12 per group
663 8-week diabetic rat hearts and their age-matched Controls).

664

Tables

Table 1

Parameter	Control (n=12)	Diabetic (n=12)
Body weight (g)	482 ± 7	299 ± 13 ***
Heart weight (g)	1.21 ± 0.04	0.96 ± 0.03 ***
Lung weight (g)	1.66 ± 0.06	1.40 ± 0.05 **
Heart weight/Body weight (%)	0.250 ± 0.007	0.326 ± 0.013 ***
Lung weight/Body weight (%)	0.343 ± 0.010	0.471 ± 0.013 ***
LV wall thickness (mm)	3.63 ± 0.16	3.54 ± 0.14
RV wall thickness (mm)	1.13 ± 0.01	1.03 ± 0.02 *
LV/RV	3.23 ± 0.16	3.45 ± 0.16
LV thickness/heart weight (mm/g)	3.02 ± 0.13	3.73 ± 0.17 ***
Blood glucose (mM)	6.8 ± 0.2	28.3 ± 1.0***
Tibia length (mm)	46.1 ± 0.3	42.0 ± 0.5 ***
LV thickness/Tibia length (%)	8.0 ± 0.4	8.4 ± 0.3

Table 1: Average heart dimensions and functional parameters of the Control and Diabetic rats used in this study. Values are mean ± SE. Student's t-tests were used to test for statistical significance (n = 12 per group, * $P < 0.05$, ** $P < 0.01$, *** $P < 0.005$).

Table 2

	RCR CI+II	UCR	FCR	CCO /OXPHOS	%CII /OXPHOS
Control	4.02±0.18	0.94±0.07	3.82±0.25	1.13±0.06	18.56±0.81
Diabetic	3.87±0.24	0.78±0.06	3.27±0.30**	1.40±0.05	14.73±0.69 **

Table 2: Mitochondrial respiratory flux control ratios. Data are from the ROS assay. RCR CI+II represents respiratory control ratios determined with CI substrates and CII with and without ADP (from the ATP assay). UCR (ETS/OXPHOS) values are an index of the respirational flux in the uncoupled state relative to the phosphorylating state. FCR or ETS/Oli ratio represents the fractional increase of ETS flux following uncoupling with FCCP from the Leak respiration state induced through inhibition of the F_1/F_0 ATP synthase oligomycin. CCO/OXPHOS ratio refers to activity of cytochrome C-oxidase (complex IV) relative to the coupled OXPHOS state. %CII/OXPHOS refers to the contribution of CII derived flux relative to overall OXPHOS. Paired student t-tests were used to test for significant differences between the Control and Diabetic groups (n = 12 per group, ** $P < 0.01$).

(a)

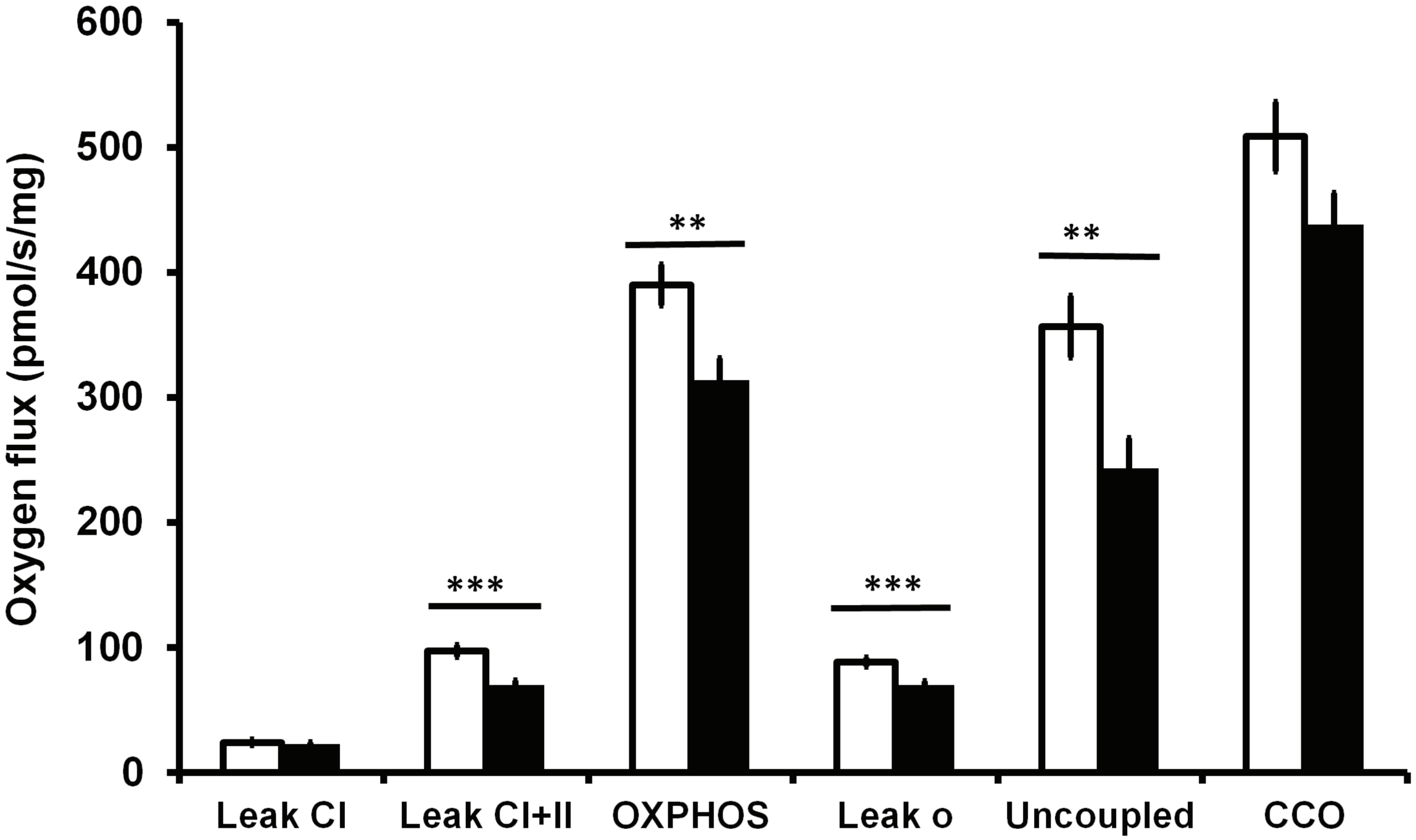
Oxygen flux (pmol/s/mg)
600
500
400
300
200
100
0
**
***
**
***
Leak CI
Leak CI+II
OXPHOS
Leak o
Uncoupled
CCO

(b)

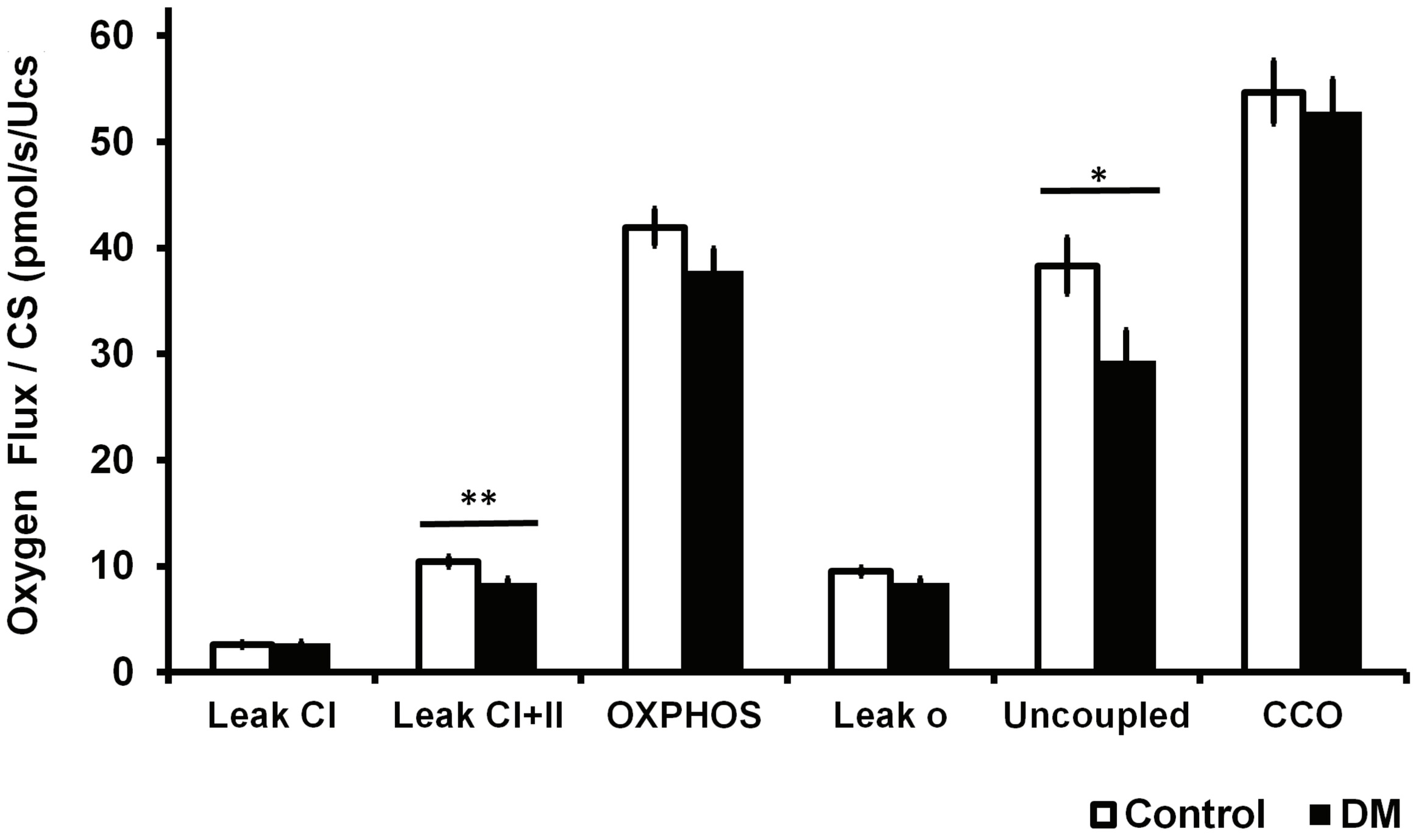
Oxygen Flux / CS (pmol/s/Ucs
60
50
40
30
20
10
0
**
*
Leak CI
Leak CI+II
OXPHOS
Leak o
Uncoupled
CCO
Control
DM

(a)

ATP Concentration (nmol/mL)

9000
7500
6000
4500
3000
1500
0
-1500
-3000

ATP Production Rate (pmol/s/mg)

3000
2500
2000
1500
1000
500
0
-500
-1000

GMP
S
ADP
Calibration reference point
Oli

5
10
15
20

Time (min)

(b)

ATP Production Rate (pmol/s/mg)

2500
2000
1500
1000
500
0
-500
-1000
-1500

***

Normoxia
Anoxia

(c)

[ATP]/[O]

2.5
2
1.5
1
0.5
0

*

OXPHOS

Control
DM

(a)

Mitochondrial membrane potential (mV)

-150
-160
-170
-180
-190
-200
-210
-220

Leak
OXPHOS
OXPHOS(d)

(b)

Time (s)

160
120
80
40
0

*

Leak-OXPHOS transition time

Control
DM

(a)

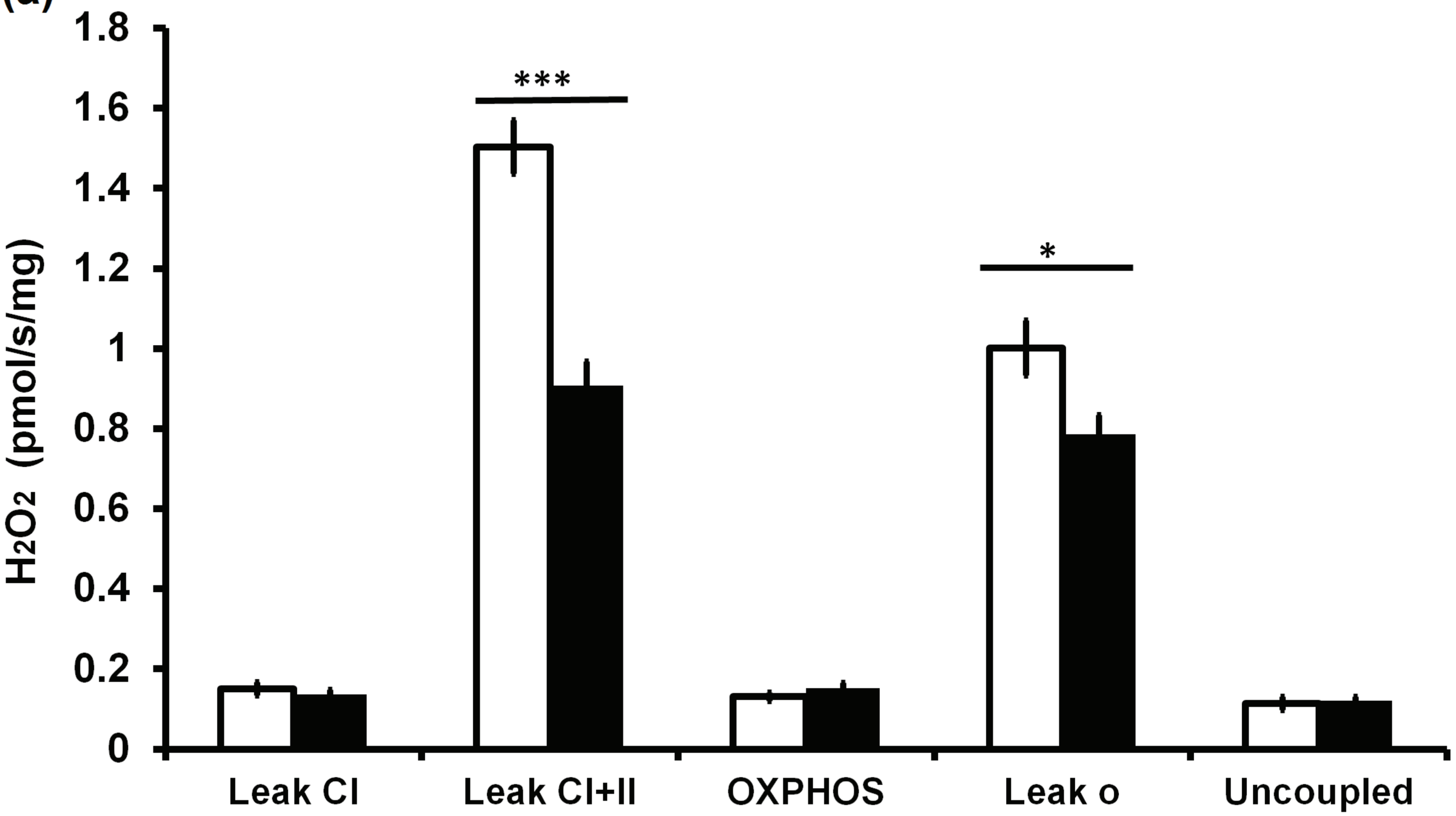
1.8
1.6
1.4
1.2
1
0.8
0.6
0.4
0.2
0
H2O2 (pmol/s/mg)
***
*
Leak CI
Leak CI+II
OXPHOS
Leak o
Uncoupled

(b)

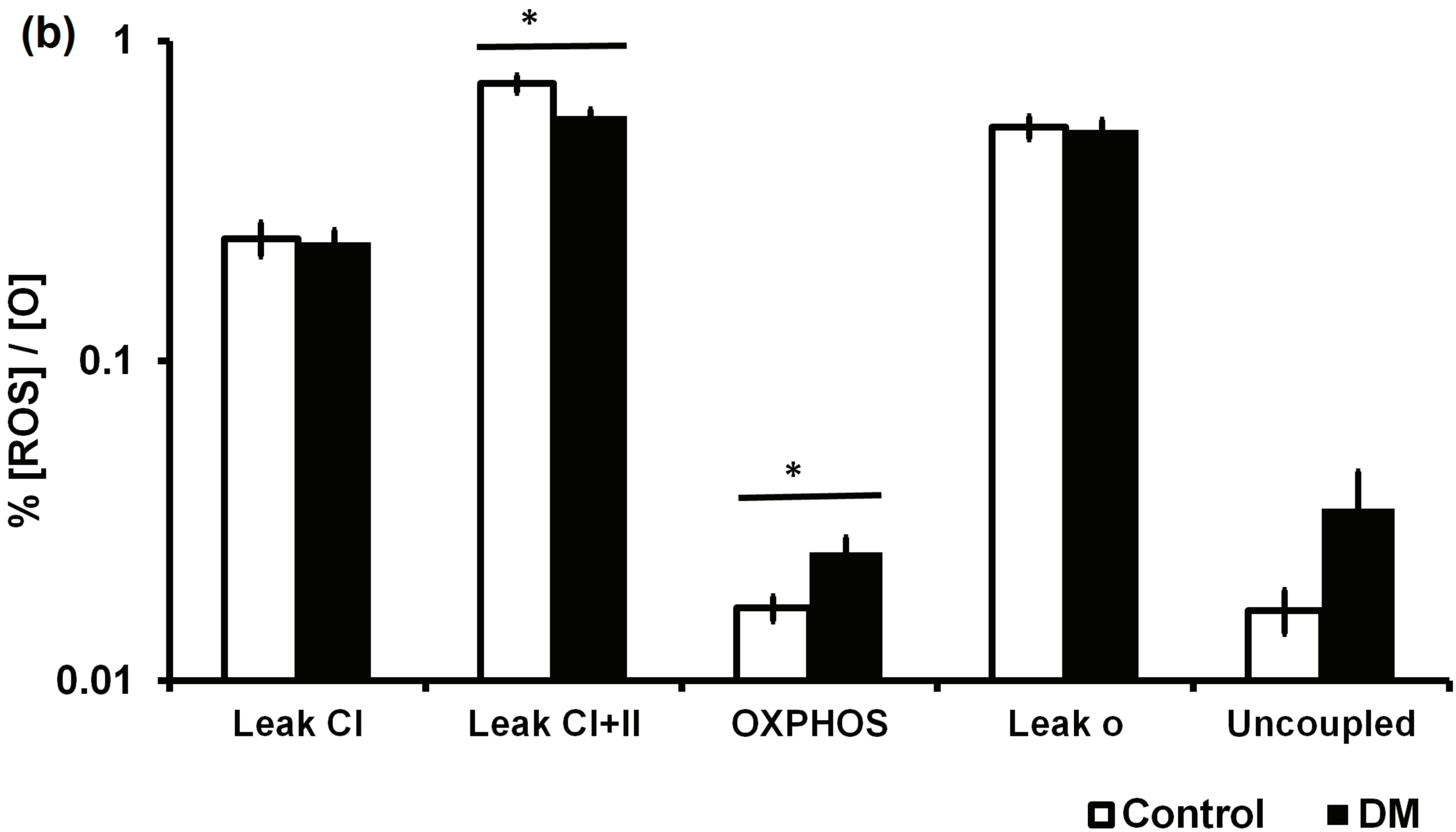
1
0.1
0.01
% [ROS] / [O]
*
*
Leak CI
Leak CI+II
OXPHOS
Leak o
Uncoupled
Control
DM